

Effects of third-neighbor interactions on the frustrated quantum Ising modelM. Roos , I. F. Muhl , and M. Schmidt ^{*}*Departamento de Física, Universidade Federal de Santa Maria, 97105-900 Santa Maria, Rio Grande do Sul, Brazil*

C. V. Morais

*Instituto de Física e Matemática - Universidade Federal de Pelotas, 96010-900 Pelotas, Rio Grande do Sul, Brazil*F. M. Zimmer *Instituto de Física, Universidade Federal de Mato Grosso do Sul, 79070-900 Campo Grande, Mato Grosso do Sul, Brazil*

(Received 6 September 2023; accepted 22 November 2023; published 30 January 2024)

We investigate thermal and quantum phase transitions of the J_1 - J_2 - J_3 transverse Ising model on the square lattice. The model is studied within a cluster mean-field decoupling, which allows us to describe phase diagrams and the free-energy landscape in the neighborhood of phase transitions. Our findings indicate that the third-neighbor coupling (J_3) can affect the nature of phase transitions of the model. In particular, ferromagnetic third-neighbor couplings favor the onset of continuous order-disorder phase transitions, eliminating the tricritical point of the superantiferromagnetic-paramagnetic (SAFM-PM) phase boundary. On the other hand, the enhancement of frustration introduced by weak antiferromagnetic J_3 gives rise to the staggered dimer phase favoring the onset of discontinuous classical phase transitions. Moreover, we find that quantum annealed criticality (QAC), which takes place when the classical discontinuous phase transition becomes critical by the enhancement of quantum fluctuations introduced by the transverse magnetic field, is eliminated from the SAFM-PM phase boundary by a relatively weak ferromagnetic J_3 . Nevertheless, this change in the nature of phase transitions can still be observed in the presence of antiferromagnetic third-neighbor couplings being also found in the staggered-dimer phase boundary. Therefore, our findings support that QAC persists under the presence of frustrated antiferromagnetic third-neighbor couplings and is suppressed when these couplings are ferromagnetic, suggesting that frustration plays a central role in the onset of QAC.

DOI: [10.1103/PhysRevE.109.014144](https://doi.org/10.1103/PhysRevE.109.014144)**I. INTRODUCTION**

Quantum phase transitions have attracted an enormous interest in the past few decades due to the exciting new physics associated with this class of phenomena [1–6]. Particular attention has been devoted to the study of the signatures of quantum criticality at finite temperature and the underlying quantum critical points at absolute zero [7,8]. Central to the understanding of these subjects is the investigation of the interplay of quantum and thermal fluctuations and the role of interactions on the emergent phase transitions. In this context, systems that exhibit classical continuous phase transitions driven by temperature can be considered candidates to study quantum criticality by tuning a nonthermal parameter, such as an external magnetic field, pressure, or chemical doping. However, the presence of classical discontinuous phase transitions still allows the onset of quantum criticality associated with a continuous phase transition at absolute zero. In this case, quantum fluctuations drive not only a ground-state phase transition but also criticality. Thus, tuning a nonthermal parameter can introduce a change in the nature of phase transitions, dubbed quantum annealed criticality (QAC). This

phenomenon is found in several compressible ferroelectric compounds [9]. In a recent contribution, a theoretical framework was developed in the context of compressible insulating systems and the possibility of QAC in other classes of many-body systems, such as multiferroics [10], has been inferred [11]. Therefore, the fundamental mechanisms concerning this phenomenon beyond the context of compressible systems is a subject worth exploring.

Recent investigations indicate that the frustrated Ising model with antiferromagnetic (AFM) interactions between first (J_1) and second neighbors (J_2) on the square lattice can exhibit QAC induced by a transverse magnetic field [12,13]. At zero field, second-neighbor couplings drive a superantiferromagnetic (SAFM) ground-state for $g = J_2/J_1 \geq 0.5$. The classical phase transitions between SAFM and the paramagnetic (PM) phases have been the subject of numerous investigations [14–20]. State-of-the-art Monte Carlo simulations for the classical model indicate that the phase boundary between SAFM and PM phases exhibits a classical tricritical point at $g_c^* = 0.67 \pm 0.01$ [18–20]. Therefore, thermal fluctuations can drive discontinuous SAFM-PM phase transitions for $0.5 \leq g < g_c^*$. Recent results from cluster mean-field (CMF) [12] and quantum cluster variational [13] methods indicate that, for a certain range of g , the classical SAFM-PM discontinuous phase transition becomes a continuous phase

^{*}mateus.schmidt@ufsm.br

transition as the transverse magnetic field is increased. In addition, series expansion calculations for the ground-state phase diagram of the quantum counterpart of the model show that continuous quantum phase transitions take place for $g < 0.67$, suggesting that the coupling coordinate of the quantum tricritical point (g_c^*) is smaller than the classical one [21]. Therefore, several results in literature suggests that criticality is driven by quantum fluctuations in the J_1 - J_2 Ising model, making it prototypical for the study of QAC.

Several recent studies indicate that the presence of other interactions in the antiferromagnetic J_1 - J_2 Ising model can alter its phase diagram [22–26]. For instance, third-neighbor interactions (J_3) can modulate the critical behavior of the system, displacing the tricritical point at the SAFM-PM phase boundary. Results from Monte Carlo simulations indicate that g_c^* is displaced towards higher values as the strength of the antiferromagnetic J_3 couplings is increased [26]. In addition, the staggered dimer (SD) phase, in which the system exhibits a pattern with antialigned pairs of aligned spins, can take place at weak antiferromagnetic third-neighbor couplings. Monte Carlo and numerical transfer matrix data suggest that a discontinuous transition separates SD and PM phases [26,27]. On the other hand, ferromagnetic J_3 favors the AFM and SAFM long-range orders, increasing its transition temperatures [26,28]. Moreover, a very recent mean-field study indicated that antiferromagnetic interactions can introduce a complex scenario concerning the order-disorder phase transitions of the model [29]. Therefore, the effects of the third-neighbor coupling on classical criticality suggests that this interaction can be relevant to the onset of QAC on the frustrated quantum Ising model. In spite of the remarkable features of the J_1 - J_2 - J_3 Ising model on the square lattice, there is an open question as to the effects of a transverse magnetic field on this model.

In this paper, we present a detailed investigation of the effects of third-neighbor interactions on the frustrated square lattice with Ising spins in the presence of a magnetic transverse field. The main goal of the present work is to identify the role of further neighbor interactions on the QAC phenomenon. We note that third-neighbor interactions can play a significant role in the behavior of magnetic systems, but its strength is often weaker than the interactions between nearest neighbors (see, for instance, Refs. [30–32]). Therefore, we constrain our analysis to $-0.4 \leq J_3/J_1 \leq 0.4$. We remark that it has been suggested that competing interactions can play a relevant role on the onset of QAC [12]. In the presence of weak AFM J_3 , a scenario of strong competition between phases and interactions takes place, providing an interesting context for the study of the QAC phenomenon. In order to investigate the J_1 - J_2 - J_3 transverse Ising model, we carried CMF calculations, providing an estimate for the system's free energy from which the nature of phase transitions can be identified. It is worth stressing that this methodology has been wielded in the study of frustrated quantum spin Hamiltonians, often providing an accurate description of phase boundaries [33–39]. For instance, the method delivers a very precise estimate for the coupling coordinate of the tricritical point at the SAFM-PM phase boundary of the J_1 - J_2 Ising model on the square lattice, $g_c^* \approx 0.66$, in strong agreement with state-of-the-art Monte Carlo simulations [20]. This theoretical framework also incorporates quantum fluctuations by exact

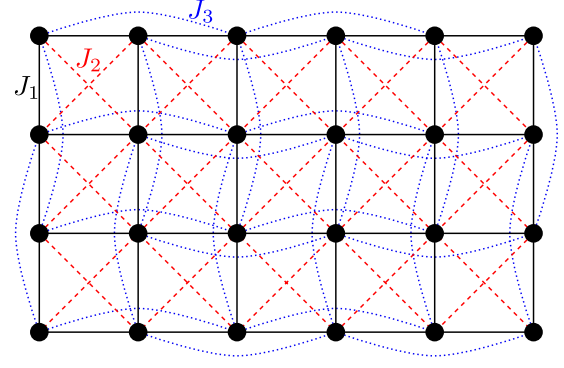


FIG. 1. Representation of the square lattice with first-neighbor (solid black), second-neighbor (dashed red), and third-neighbor (dotted blue) interactions.

diagonalization of the intracluster terms, which allowed the QAC in the J_1 - J_2 quantum Ising model to be identified [12]. Therefore, the CMF method can provide important insight into the role of frustration and quantum fluctuations in the phase transitions hosted by the J_1 - J_2 - J_3 quantum Ising model.

This paper is organized as follows. In Sec. II, the energies associated with the ordered phases in the absence of both quantum and thermal fluctuations are discussed. In addition, the CMF approach for each phase is presented. Phase diagrams and a detailed description of the free-energy landscape are provided in Sec. III, where the effects of couplings, temperature, and the transverse field on the present model are described. Finally, a conclusion is given in Sec. IV.

II. MODEL AND METHOD

The Hamiltonian of the transverse Ising model is given by

$$\mathcal{H} = \sum_{i,j} J_{ij} \sigma_i^z \sigma_j^z - \Gamma \sum_i \sigma_i^x, \quad (1)$$

where J_{ij} is the exchange coupling between pairs of spins at the vertices of a square lattice (see Fig. 1) and Γ is the transverse magnetic field. Here, σ_i^z and σ_i^x denote the z and x components of the Pauli spin matrices, respectively. In the present work, we adopt antiferromagnetic interactions between first and second neighbors, i.e., $J_1 > 0$ and $J_2 > 0$. In addition, we investigate the cases in which the third-neighbor interactions can be ferromagnetic and antiferromagnetic, allowing $|J_3| \leq 0.4J_1$.

In the zero-field limit of this model, three different ordered phases can be found for the set of parameters adopted in the present work. A Néel antiferromagnet, as illustrated in Fig. 2(a), with a ground-state energy per spin of $U_{\text{AFM}} = -2J_1 + 2J_2 + 2J_3$, can be found when first-neighbor interactions are dominant. Strong second-neighbor interactions can lead to the SAFM state, which is shown in Fig. 2(b). In this phase, all second-neighbor interactions are satisfied, while first-neighbor interactions are partially frustrated and the third-neighbor interactions are fully frustrated, leading to the ground-state energy per spin $U_{\text{SAFM}} = -2J_2 + 2J_3$. At weak AFM third-neighbor interactions the system can exhibit the SD phase, in which 1/4 of the AFM first-neighbor interactions and 1/2 of the second- and third-neighbor couplings

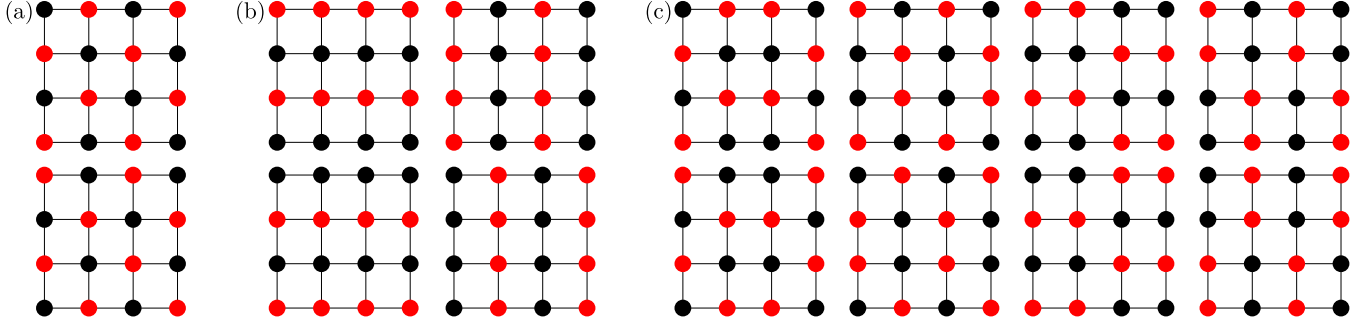


FIG. 2. Schematic view of spin configurations of the phases (a) AFM, (b) SAFM, and (c) SD. Red and black circles represent spins up and down, respectively. Configurations in lower panels are obtained by global spin inversion of the configurations in upper panels.

are frustrated. This phase exhibits an eightfold degeneracy, as shown in Fig. 2(c), and a ground-state energy of $U_{\text{SD}} = -J_1$. By comparing the ground-state energies of the different phases, one can evaluate the ground-state phase diagram of the present model.

In the presence of thermal and quantum fluctuations, the exact free energy of this model is not available and one needs to consider numerical and/or analytical approximations in order to describe its phase transitions. In the present work, we adopt a CMF approach, which has been employed in the study of several spin models with competing interactions [24,40–47], including the J_1 - J_2 quantum Ising model on the square lattice [12,48]. In this method, the system is divided into clusters capable of exhibiting a repeating pattern. The interactions within the clusters are treated exactly, while the couplings between clusters are evaluated following the standard mean-field approximation $\sigma_i^z \sigma_j^z \approx m_i^z \sigma_j^z + \sigma_i^z m_j^z - m_i^z m_j^z$, where m_i^z is the z component of the magnetization of site i . Here, we consider a four-site cluster, which is known to provide an estimate for the tricritical point in the SAFM-PM phase boundary for the J_1 - J_2 Ising model in excellent agreement with Monte Carlo simulations [12,20,48]. Therefore, this approximation provides a starting point to introduce both quantum fluctuations and third-neighbor interactions in the model.

Within the CMF approximation, the single-cluster Hamiltonian is given by

$$\mathcal{H}_{\text{CMF}} = \mathcal{H}_0 + \mathcal{H}_{\text{MF}} - \Gamma \sum_{i=1}^4 \sigma_i^x, \quad (2)$$

with

$$\mathcal{H}_0 = J_1(\sigma_1^z + \sigma_4^z)(\sigma_2^z + \sigma_3^z) + J_2(\sigma_1^z \sigma_4^z + \sigma_2^z \sigma_3^z) \quad (3)$$

containing the intracluster terms and \mathcal{H}_{MF} incorporating the mean-field contribution. This term is a function of the local magnetizations

$$m_i^z = \langle \sigma_i^z \rangle = \frac{\text{Tr} \sigma_i^z e^{-\beta \mathcal{H}_{\text{CMF}}}}{\text{Tr} e^{-\beta \mathcal{H}_{\text{CMF}}}}, \quad (4)$$

where $\beta = 1/k_B T$, in which T is the temperature and k_B is the Boltzmann constant. Within the present four-site approximation, one can relate the local magnetizations from different sites and clusters in a straightforward way that depends only on the particular phase under study. Therefore, the CMF Hamiltonian can be written as a function of a single

local magnetization; here m_1^z is chosen as the independent parameter.

For the AFM phase, as shown in Fig. 2(a), the clusters exhibit the same magnetization pattern and within each cluster the local magnetizations respect the relation $m_1^z = -m_2^z = -m_3^z = m_4^z$. Thereby, the intercluster Hamiltonian for this phase can be written as

$$\mathcal{H}_{\text{MF}}^{\text{AFM}} = (-2J_1 + 3J_2 + 4J_3)m_1^z \lambda_{\text{AFM}}, \quad (5)$$

where

$$\lambda_{\text{AFM}} = \sigma_1^z - \sigma_2^z - \sigma_3^z + \sigma_4^z - 2m_1^z. \quad (6)$$

For the SAFM phase, there are four equivalent magnetization patterns, which are shown in Fig. 2(b). In the present approach, we consider the magnetization patterns with antialigned columns of spins, for which $m_1^z = -m_2^z = m_3^z = -m_4^z$. Then, the intercluster Hamiltonian is given by

$$\mathcal{H}_{\text{MF}}^{\text{SAFM}} = (-3J_2 + 4J_3)m_1^z \lambda_{\text{SAFM}}, \quad (7)$$

where

$$\lambda_{\text{SAFM}} = \sigma_1^z - \sigma_2^z + \sigma_3^z - \sigma_4^z - 2m_1^z. \quad (8)$$

It is worth stressing that this particular choice of the magnetization pattern with columns provides equivalent results when considering the other two possibilities depicted in Fig. 2(b) [23].

For the SD phase, there are eight possible ground-states, as shown in Fig. 2(c). We note that the ground-state energy of this phase depends only on J_1 and, therefore, we consider the configurations that leads to more frustrated J_1 interactions within the cluster. In this way, frustration effects that could be relevant for the phase transitions are incorporated by exact diagonalization instead of the mean-field decoupling. The SD configuration that leads to more frustrated first-neighbor intracluster couplings is the one depicted in Fig. 3. In this case, the local magnetizations can exhibit different patterns within different clusters. In particular, cluster v' exhibits the same local magnetization pattern of the central cluster v . On the other hand, cluster v'' exhibits a local magnetization pattern in which equivalent sites from v show a magnetization with the opposite sign. It means that $m_i^z = m_{v'}^z = -m_{v''}^z$, allowing us to write the local magnetization from different clusters in terms of the central one.

Within the central cluster v , $m_1^z = m_2^z = -m_3^z = -m_4^z$ and, therefore, the MF contribution within the SD phase is given

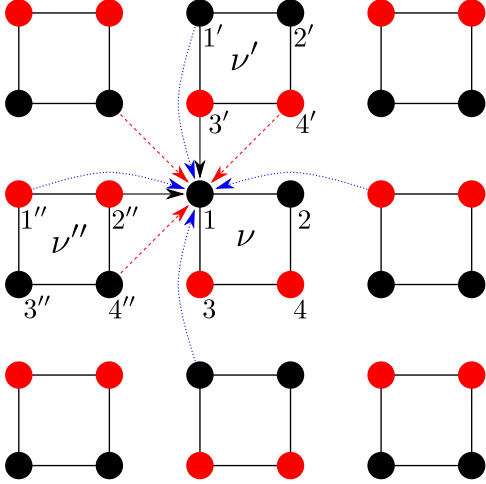


FIG. 3. The square lattice divided into four-site clusters within the CMF approximation, with intracluster interactions J_1 represented by solid lines. The mean fields are represented by arrows only for the site 1 of the central cluster ν . Solid circles indicate the local magnetization pattern consistent with the SD phase.

by

$$\mathcal{H}_{\text{MF}}^{\text{SD}} = (-2J_1 + J_2)m_1^z \lambda_{\text{SD}}, \quad (9)$$

where

$$\lambda_{\text{SD}} = \sigma_1^z + \sigma_2^z - \sigma_3^z - \sigma_4^z - 2m_1^z. \quad (10)$$

In order to investigate the J_1 - J_2 - J_3 Ising model, the single-cluster problem given by Eq. (2) and the local magnetization $m_1^z = \langle \sigma_1^z \rangle$ should be solved in a self-consistent way. The mean-field term \mathcal{H}_{MF} should be adopted accordingly with the phase under consideration; i.e., for the AFM, SAFM, and SD phases, one must consider Eqs. (5), (7), and (9), respectively. After solving the CMF Hamiltonian, one can compute the system's free energy per cluster,

$$F = -k_B T \ln \text{Tre}^{-\beta \mathcal{H}_{\text{CMF}}}, \quad (11)$$

for each phase. The order parameter of each phase can be evaluated from the equations

$$\begin{aligned} m_{\text{AFM}} &= (m_1^z - m_2^z - m_3^z + m_4^z)/4, \\ m_{\text{SAFM}} &= (m_1^z - m_2^z + m_3^z - m_4^z)/4, \quad \text{and} \\ m_{\text{SD}} &= (m_1^z + m_2^z - m_3^z - m_4^z)/4. \end{aligned} \quad (12)$$

III. RESULTS

In this section, we present our numerical results within the CMF approximation. The phase transitions are investigated by computing the order parameter and the free-energy of each phase. We discuss the phase transitions in terms of the free-energy landscape, by evaluating the free energy per cluster as a function of the order parameter. Within our calculations, the local magnetization m_1^z is equivalent to the order parameter and, therefore, the behavior of $F(m_1^z)$ allows us to describe the nature of phase transitions. For numerical purposes, we adopt $k_B = 1$. The first-neighbor interaction (J_1) is taken as the energy unit. The second-neighbor interaction is constrained to

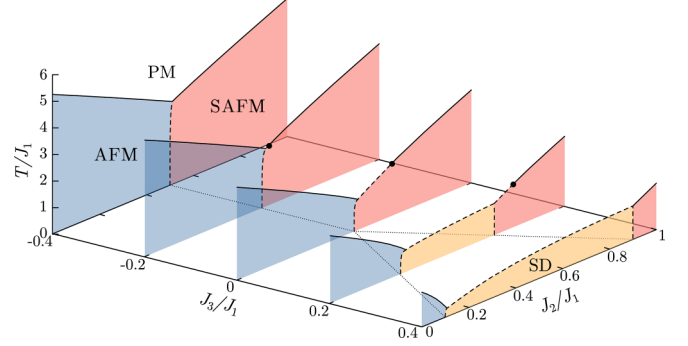


FIG. 4. Classical phase diagram ($\Gamma = 0$) of the frustrated square lattice. Solid and dashed lines represent continuous and discontinuous phase transitions respectively. Solid circles indicate the tricritical point. Dotted lines indicate the ground-state boundaries between the ordered phases.

a positive value not larger than the first-neighbor coupling. We also consider the relatively weak third-neighbor interactions $-0.4 \leq J_3/J_1 \leq 0.4$.

A. Classical phase diagram

In Fig. 4, the classical phase diagram of the J_1 - J_2 - J_3 Ising model is presented. In the absence of third-neighbor interactions, the coupling-temperature (J_2/J_1 - T/J_1) phase diagram exhibits a tricritical point in the PM-SAFM phase boundary at $J_2/J_1 \approx 0.66$. This result is in agreement with several others' CMF implementations [12,20,48,49] and is in very good agreement with state-of-the-art Monte Carlo simulations that predict a tricritical point at $J_2/J_1 \approx 0.67 \pm 0.01$ [18]. The presence of ferromagnetic $J_3 < 0$ interactions favors AFM and SAFM long-range orders, increasing the transition temperatures of these phases. For weak third-neighbor interactions, the structure of the phase diagram is the same as that for $J_3 = 0$. For instance, for $J_3/J_1 = -0.2$, the AFM-PM phase transitions are continuous and a tricritical point can be observed in the SAFM-PM phase boundary. It is worth noting that the range of J_2/J_1 in which discontinuous SAFM-PM phase transitions take place is reduced with the increase of the ferromagnetic third-neighbor interactions. As a consequence, the tricritical point is displaced towards $J_2/J_1 = 0.5$. For a strong enough ferromagnetic J_3 coupling, the tricritical point vanishes and all order-disorder phase transitions become continuous, as shown for $J_3/J_1 = -0.4$. Therefore, our findings suggest that ferromagnetic third-neighbor couplings are able to increase the ordering temperature and suppress first-order phase transitions in the temperature-coupling phase diagram of the model. We remark that Monte Carlo simulations for the present model indicated that the ordering temperature of the SAFM-PM phase transitions is enhanced by an increasing magnitude of the ferromagnetic J_3 coupling [26], corroborating our findings.

The presence of antiferromagnetic third-neighbor couplings ($J_3 > 0$) introduces an additional source of frustration in the model. This coupling is not satisfied within the microscopic configurations of the AFM and SAFM phases, increasing its ground-state energy. Thus, the AFM-PM and SAFM-PM transition temperatures are reduced by the

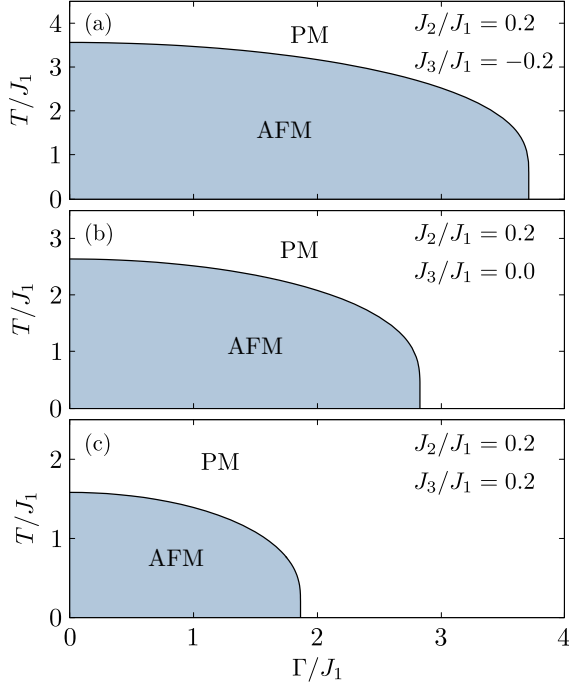


FIG. 5. Field-temperature phase diagram for $J_2/J_1 = 0.2$ and for (a) ferromagnetic ($J_3/J_1 = -0.2$) third-neighbor couplings, (b) in the absence of J_3 and (c) in the presence of antiferromagnetic ($J_3/J_1 = 0.2$) third-neighbor couplings. Solid lines indicate continuous phase transitions.

increase in the antiferromagnetic J_3 coupling. Moreover, antiferromagnetic third-neighbor interactions drive the onset of the degenerated SD phase near $J_2/J_1 \approx 0.5$. In fact, the range of J_2/J_1 in which the SD phase arises is proportional to J_3/J_1 . In the range of J_3/J_1 considered in this work, the classical SD-PM transitions are discontinuous. This result is in agreement with Monte Carlo simulations [26,28], which indicates a strong first-order phase transition between SD and PM phases. We also note that the coupling coordinate of the tricritical point is displaced to higher values, as can be noted for $J_3/J_1 = 0.2$. It is worth remarking that this displacement in g_c^* is also observed in Monte Carlo outcomes [26]. Therefore, our findings for the effects of third-neighbor couplings on the classical J_1 - J_2 - J_3 Ising model are in fair agreement with recent Monte Carlo results.

B. Phase transitions under a transverse field

The presence of a finite transverse magnetic field introduces quantum fluctuations on the J_1 - J_2 - J_3 Ising model. Our findings indicate that the effects of these quantum fluctuations are determined by the strength of exchange couplings. Although a strong enough transverse field can suppress any magnetic long-range order, driving a polarized PM state, its effect on the nature of phase transitions depends strongly on the phases under transformation.

In Fig. 5, temperature *versus* transverse-field phase diagrams for $J_2/J_1 = 0.2$ depict quantum phase transitions from the AFM to PM state at a critical transverse field. The presence of ferromagnetic third-neighbor interactions increases the

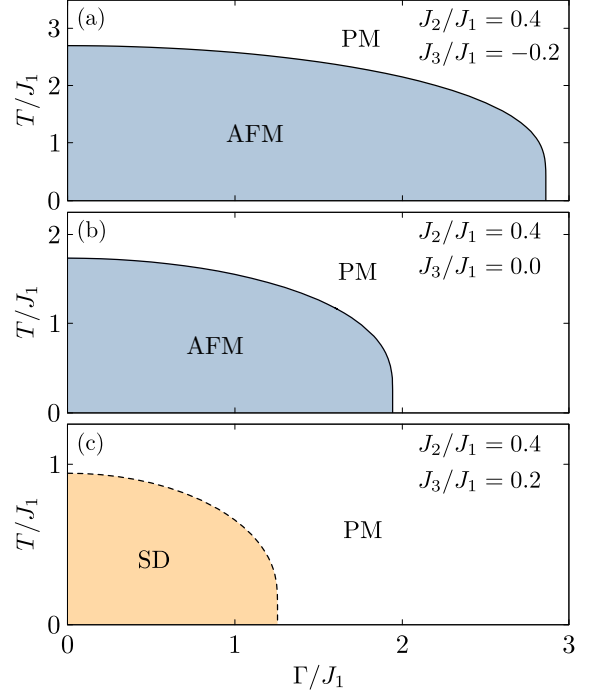


FIG. 6. Field-temperature phase diagram for $J_2/J_1 = 0.4$ and for (a) ferromagnetic ($J_3/J_1 = -0.2$) third-neighbor couplings, (b) in the absence of J_3 and (c) in the presence of antiferromagnetic ($J_3/J_1 = 0.2$) third-neighbor couplings. The same convention of Fig. 4 was adopted.

critical transverse field, as noted by comparing Figs. 5(a) and 5(b). On the other hand, an antiferromagnetic J_3 coupling reduces the critical transverse field of the AFM-PM phase transition, as shown in Fig. 5(c) for $J_3/J_1 = 0.2$. Although the location of phase transitions is affected by weak third-neighbor couplings, their nature remains the same. In other words, even in the presence of weak third-neighbor interactions ($J_3/J_1 = \pm 0.2$), the system exhibits only continuous phase transitions between AFM and PM phases.

Another interesting scenario arises for $J_2/J_1 = 0.4$ (Fig. 6), which is close to the AFM-SAFM ground-state phase boundary for $J_3/J_1 \leq 0$ and can lead to the SD phase for $J_3/J_1 > 0$. While the AFM-PM phase boundary exhibits only continuous phase transitions for $J_3/J_1 = 0$ and -0.2 , discontinuous phase transitions can be found in the whole SD-PM phase boundary for $J_3/J_1 = 0.2$. Therefore, our results indicate that the transverse field alone is unable to change the nature of phase transitions for $J_2/J_1 < 0.5$.

Our findings support that a rich scenario is introduced by quantum fluctuations when $J_2/J_1 > 0.5$. For $J_2/J_1 = 0.6$, the nature of phase transitions is strongly dependent on the strength of the third-neighbor interactions and the transverse field (see Fig. 7). Strong enough third-neighbor ferromagnetic interactions introduce continuous classical phase transitions. As shown in Fig. 7(a), this SAFM-PM transition remains continuous when the transverse field is increased. However, in the presence of antiferromagnetic third-neighbor interactions, the SD-PM phase boundary arises, exhibiting only first-order phase transitions [see Fig. 7(c)]. Nevertheless, for $J_3/J_1 = 0$, the nature of the SAFM-PM phase boundary is

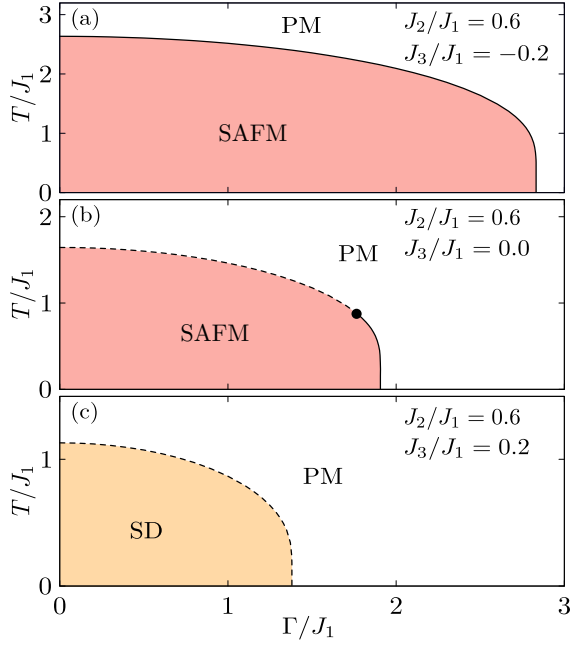


FIG. 7. Field-temperature phase diagram for $J_2/J_1 = 0.6$ and for (a) ferromagnetic ($J_3/J_1 = -0.2$) third-neighbor couplings, (b) in the absence of J_3 and (c) in the presence of antiferromagnetic ($J_3/J_1 = 0.2$) third-neighbor couplings. The same convention of Fig. 4 was adopted.

strongly dependent on the transverse-field strength, as reported in Ref. [12]. For weak transverse fields, a discontinuous SAFM-PM phase transition is obtained [see Fig. 7(b)]. At this phase transition, the free-energy landscape reveals three minima near the order-disorder phase transition, as shown in Fig. 8(a) for $\Gamma/J_1 = 1$. Two of these minima occur at finite values of m_1^z , equidistant from 0, corresponding to the ordered SAFM solution. Below the ordering temperature (i.e., $T/J_1 = 1.4590$), the free energy of the SAFM solution is lower than that of the PM solution ($m_1^z = 0$). At the ordering temperature, the three minima exhibit the same value, as illustrated for $T/J_1 = 1.4597$. Just above the ordering temperature ($T/J_1 = 1.4610$), the paramagnetic solution shows the lowest free energy, but the local minima associated with the SAFM solution are still present. Increasing the transverse-field strength leads to a change in the nature of phase transitions, as indicated by the tricritical point in the phase diagram. Near tricriticality, the free energy becomes more sensitive to thermal fluctuations. In Fig. 8(b), the free-energy landscape for $\Gamma/J_1 = 1.75$ is shown. Although the system undergoes a first-order phase transition, with three minima observed below and at the ordering temperature, a single minimum can be observed slightly above the ordering temperature. For stronger transverse fields, continuous phase transitions can be observed, as indicated by the behavior of the free energy for $\Gamma/J_1 = 1.9$ in Fig. 8(c). Below the ordering temperature, two minima can be observed at finite values of m_1^z and the paramagnetic solution corresponds to a local maximum, which is expected near a continuous phase transition. As temperature is increased towards the transition temperature, the free-energy minima are displaced towards $m_1^z = 0$ and a flat free-energy region can be noted very close

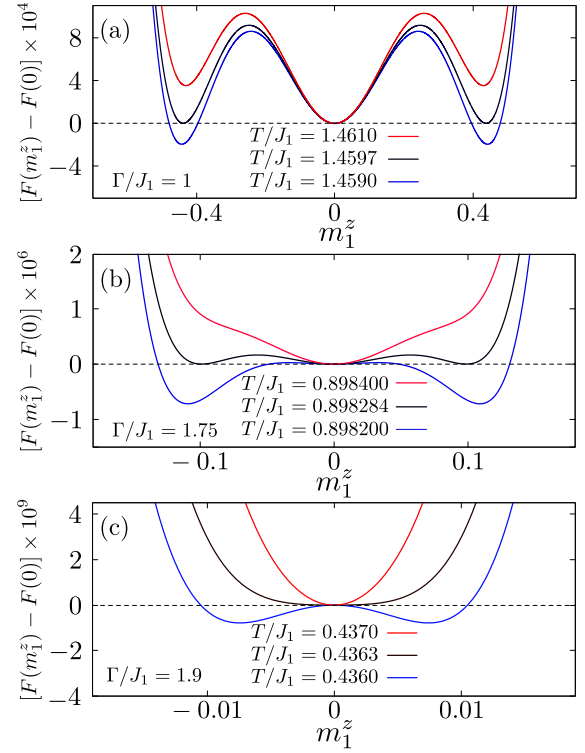


FIG. 8. Difference between the free energy per cluster as a function of the local magnetization m_1^z [$F(m_1^z)$] and the free energy per cluster of the paramagnetic phase [$F(0)$] near the ordering temperature for $J_2/J_1 = 0.6$ in the absence of third-neighbor couplings with (a) $\Gamma/J_1 = 1$ (b) $\Gamma/J_1 = 1.75$, and (c) $\Gamma/J_1 = 1.9$. The free energy is computed assuming the SAFM phase solution.

to the ordering temperature. Within the paramagnetic phase, the system exhibits a single minimum at $m_1^z = 0$. It is worth stressing that this change in the nature of phase transitions is ruled by quantum fluctuations introduced by the transverse magnetic field.

In the absence of third-neighbor interactions, the QAC phenomenon disappears for $J_2/J_1 > 0.66$, as reported in a CMF study of the J_1 - J_2 quantum Ising model [12]. This occurs due to the absence of discontinuous classical phase transitions. However, antiferromagnetic third-neighbor couplings can favor the onset of discontinuous classical phase transitions at stronger second-neighbor couplings, as shown in Fig. 4. In Fig. 9, we present the effects of antiferromagnetic third-neighbor couplings on the phase boundaries of the model for $J_2/J_1 = 0.75$. The free-energy landscape is explored in two scenarios, namely, weak quantum fluctuations and strong thermal fluctuations ($\Gamma/J_1 = 1$ near the ordering temperature) and for strong quantum fluctuations and weak thermal fluctuations ($T/J_1 = 0.4$ and near the transition transverse field). These scenarios are indicated by arrows in the phase diagrams shown in Fig. 9. For $J_3/J_1 = 0$, the free-energy landscape exhibits the signatures of continuous phase transitions at weak [Fig. 9(d)] and strong [Fig. 9(g)] transverse fields in which the nature of phase transitions is not affected by quantum fluctuations. In Fig. 9(b), first-order phase transitions occur for moderate transverse fields, such as $\Gamma/J_1 = 1$, which means that the free-energy exhibits minima associated with both

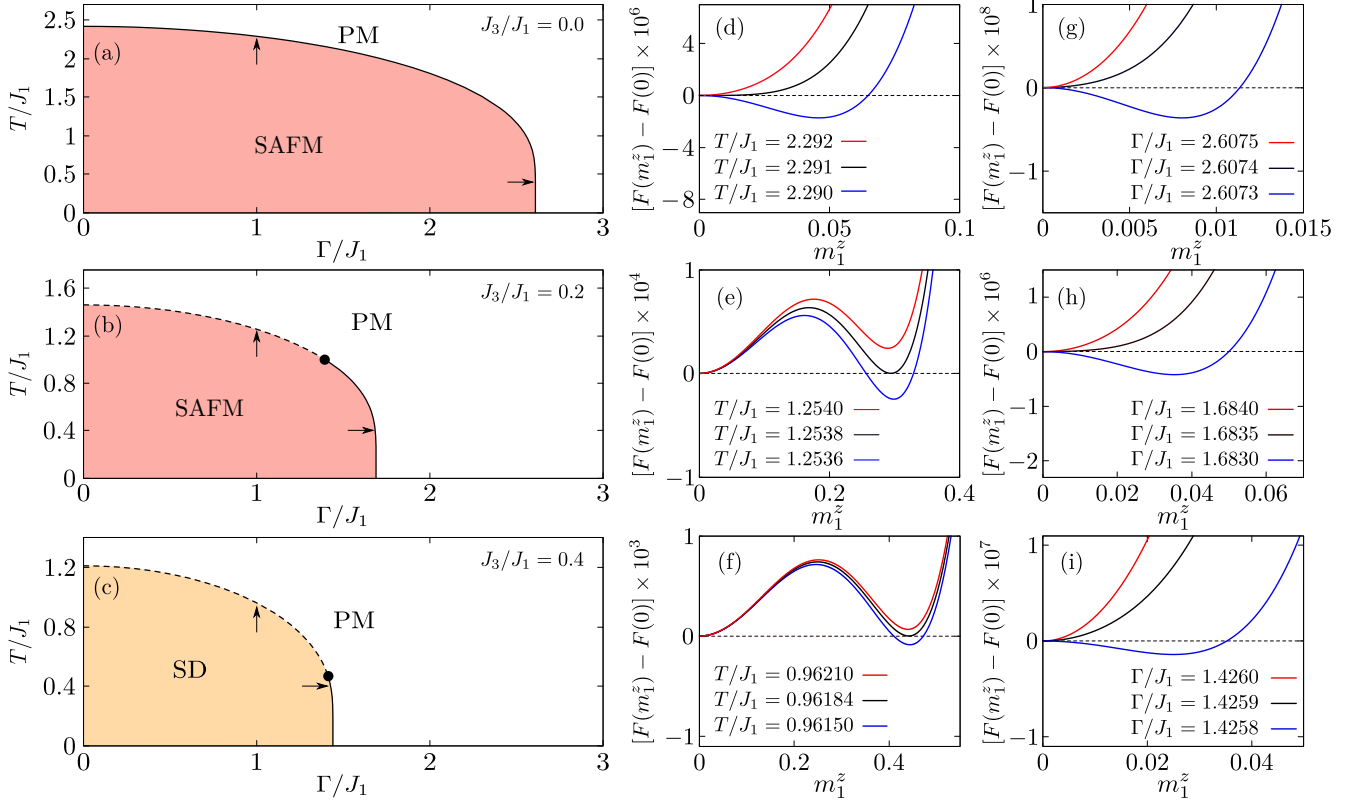


FIG. 9. Effects of third-neighbor interactions on temperature–transverse-field phase diagrams for $J_2/J_1 = 0.75$. Panels (a)–(c) exhibit phase diagrams in which the same convention of Fig. 4 was adopted. Upper and lower arrows indicate strong thermal/weak quantum and weak thermal/strong quantum fluctuations, respectively. Each phase diagram is accompanied by plots of the free-energy landscape in the right-hand side near the ordering temperature (upper arrows) for $\Gamma/J_1 = 1$ [panels (d)–(f)] and near the transition transverse field (lower arrows) for $T/J_1 = 0.4$ [panels (g)–(i)]. The free energy is obtained by adopting the solution of the ordered phase in the corresponding phase diagram.

ordered and disordered phases below the ordering temperature [see Fig. 9(e)]. At stronger transverse fields, the transition becomes continuous as can be noted by the behavior of the free energy in Fig. 9(h). Therefore, the QAC phenomenon arises in the SAFM-PM phase boundary even for $J_2/J_1 > 0.66$ when antiferromagnetic third-neighbor couplings are present. Remarkably, the same change in the nature of phase transitions can be spotted in the phase diagram and the free-energy landscape for $J_3/J_1 = 0.4$, in which a SD-PM phase transition is driven by both thermal and quantum fluctuations [see Figs. 9(c), 9(f), and 9(i)]. Therefore, our findings suggest that QAC is not restricted to the phase transitions between SAFM and PM phases in the frustrated square lattice.

In Fig. 10, we summarize our findings, providing a pictorial view of the effects of couplings on the classical and quantum phase transitions hosted by the frustrated Ising square lattice. Solid lines indicate the ground-state phase boundaries separating AFM, SAFM, and SD phases in the absence of the transverse field. In addition, the location of the classical and quantum tricritical points in the J_2/J_1 - J_3/J_1 plane allows us to identify regions in which only one type of phase transition can be driven by both temperature and transverse field. The coupling coordinates of the classical tricritical points can be obtained from temperature-coupling phase diagrams in the zero-field limit, such as those shown in Fig. 4. For the quantum tricritical points, the coupling coordinates were obtained from field-coupling phase diagrams at $T = 0$ for

several strengths of J_3/J_1 . The model exhibits only continuous transitions between AFM and PM phases driven by both thermal and quantum fluctuations. Therefore, no tricritical point

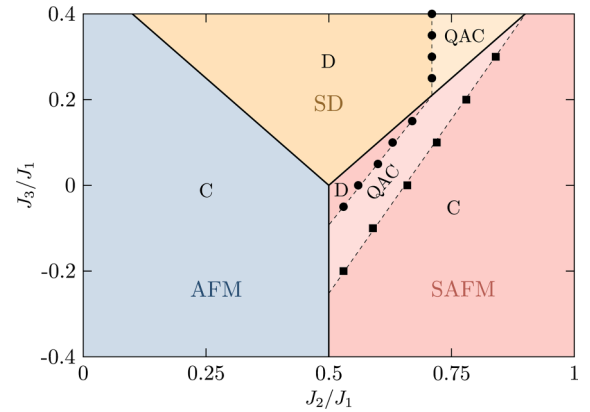


FIG. 10. The role of exchange couplings on the classical and quantum phase transitions. Solid lines delimit the zero-field ground-state phase boundaries. Solid circles and squares indicate the coupling coordinates of the quantum and classical tricritical points, respectively. Dashed lines are guides to the eye, delimiting the range of exchange parameters in which QAC (indicated by lighter colors), only continuous (C), and only discontinuous (D) phase transitions can be found.

is found in the AFM-PM phase boundary. In the SAFM-PM phase boundary, there are regions in which both thermal and quantum fluctuations drive phase transitions of the same nature. However, one can identify a region in the J_2/J_1 - J_3/J_1 plane in which classical phase transitions are discontinuous (in the left-hand side of the classical tricritical points) but the quantum phase transitions are continuous (in the right-hand side of the quantum tricritical points). In this region, which is indicated by a lighter color in Fig. 10, QAC can be found. A region in which QAC can be observed is also indicated for the SD-PM phase transition. In the range of parameters considered in the present work, only discontinuous classical phase transitions between SD and PM phases were found at zero field. On the other hand, a transverse field can drive zero-temperature continuous quantum phase transitions between these phases. Therefore, the coupling coordinates of the quantum tricritical points in the SD-PM phase boundary separate the region in which only discontinuous (quantum and classical) phase transitions are observed and the region with the emergence of QAC.

IV. CONCLUSION

We investigate the transverse-field Ising model on the square lattice with exchange interactions between first, second, and third neighbors. By employing a four-site CMF approximation, we provide a description of the effects of third-neighbor couplings and transverse fields on the nature of phase transitions, presenting phase diagrams and the free-energy landscape in the vicinity of phase transitions. In the absence of transverse fields, our findings support that ferromagnetic J_3 interactions favor AFM and SAFM phases, enhancing its ordering temperatures, and avoid discontinuous phase transitions in the SAFM-PM phase boundary, suppressing tricriticality. On the other hand, weak antiferromagnetic J_3 interactions can drive the onset of the SD phase and increase the coupling coordinate of the tricritical point found in the SAFM-PM phase boundary. These results are consistent with the Monte Carlo data from the literature [26,28].

In the presence of transverse fields, results from CMF [12] and quantum cluster variational [13] methods indicate that the J_1 - J_2 Ising model can exhibit the QAC phenomenon in the SAFM-PM phase boundary. Our analysis of phase

transitions indicates that ferromagnetic J_3 interactions suppress the onset of QAC in the model. On the other hand, our results supported by the system's free-energy landscape suggest the QAC phenomenon is robust under the presence of weak antiferromagnetic third-neighbor couplings, being also found in the SD-PM phase boundary. Therefore, our work reports on the possible onset of QAC in two different phases of the frustrated square lattice. We hope that our CMF findings motivate further investigations of the present model by means of numerical and analytical methods, such as effective-field theory [14], series expansion [21], quantum Monte Carlo [50], and quantum cluster variational [13] methods. It is also worth noting that our CMF investigation focused on the long-range orders observed in the ground-state of the model, so we cannot rule out the onset of other phases at finite temperature. In fact, a recent mean-field investigation suggests that a complex scenario of ordered phases can arise in the zero-field limit of the present model [29]. Moreover, a relevant subject concerns the onset of incommensurate phases, which have been reported for frustrated Ising spin systems [27,51–53]. An interesting question is whether these phases can arise in the J_1 - J_2 - J_3 quantum Ising model, which could be addressed by employing the numerical transfer matrix technique [27,52].

In our opinion, our findings for the frustrated quantum Ising model make this particular model a prototype for the experimental realization of QAC. It is worth noting that several two-dimensional magnets have been produced in the growing field of van der Waals materials [54], including magnets with Ising anisotropy and competing interactions [55]. Another route to the experimental observation of QAC could be the implementation of two-dimensional arrays of Rydberg atoms, which have been used to simulate the antiferromagnetic transverse-field Ising model on the square lattice [56,57]. We believe that mechanisms able to tune the interactions in these experimental systems can provide platforms for the investigation of the QAC phenomenon.

ACKNOWLEDGMENTS

This work was supported by the Brazilian agencies Conselho Nacional de Desenvolvimento Científico e Tecnológico (CNPq), Coordenação de Aperfeiçoamento de Pessoal de Nível Superior (Capes), and Fundação de Amparo à Pesquisa do Estado do Rio Grande do Sul (Fapergs).

-
- [1] S. L. Sondhi, S. M. Girvin, J. P. Carini, and D. Shahar, *Rev. Mod. Phys.* **69**, 315 (1997).
 - [2] S. Sachdev, *Phys. World* **12**, 33 (1999).
 - [3] M. Vojta, *Rep. Prog. Phys.* **66**, 2069 (2003).
 - [4] W. H. Zurek, U. Dorner, and P. Zoller, *Phys. Rev. Lett.* **95**, 105701 (2005).
 - [5] M. Brando, D. Belitz, F. M. Grosche, and T. R. Kirkpatrick, *Rev. Mod. Phys.* **88**, 025006 (2016).
 - [6] M. Heyl, *Rep. Prog. Phys.* **81**, 054001 (2018).
 - [7] S. Sachdev, *Science* **288**, 475 (2000).
 - [8] M. Vojta, *Rep. Prog. Phys.* **81**, 064501 (2018).
 - [9] P. Chandra, G. G. Lonzarich, S. E. Rowley, and J. F. Scott, *Rep. Prog. Phys.* **80**, 112502 (2017).
 - [10] A. Narayan, A. Cano, A. V. Balatsky, and N. A. Spaldin, *Nat. Mater.* **18**, 223 (2019).
 - [11] P. Chandra, P. Coleman, M. A. Continentino, and G. G. Lonzarich, *Phys. Rev. Res.* **2**, 043440 (2020).
 - [12] N. Kellermann, M. Schmidt, and F. M. Zimmer, *Phys. Rev. E* **99**, 012134 (2019).
 - [13] E. Domínguez, C. E. Lopetegui, and R. Mulet, *Phys. Rev. B* **104**, 014205 (2021).
 - [14] A. Bobák, T. Lučivjanský, M. Borovský, and M. Žukovič, *Phys. Rev. E* **91**, 032145 (2015).
 - [15] H. Li and L.-P. Yang, *Phys. Rev. E* **104**, 024118 (2021).
 - [16] V. A. Abalmasov and B. E. Vugmeister, *Phys. Rev. E* **107**, 034124 (2023).

- [17] A. Kalz, A. Honecker, and M. Moliner, *Phys. Rev. B* **84**, 174407 (2011).
- [18] S. Jin, A. Sen, and A. W. Sandvik, *Phys. Rev. Lett.* **108**, 045702 (2012).
- [19] A. Kalz and A. Honecker, *Phys. Rev. B* **86**, 134410 (2012).
- [20] S. Jin, A. Sen, W. Guo, and A. W. Sandvik, *Phys. Rev. B* **87**, 144406 (2013).
- [21] J. Oitmaa, *J. Phys. A: Math. Theor.* **53**, 085001 (2020).
- [22] Y. Xu and D.-X. Yao, *Phys. Rev. B* **97**, 224419 (2018).
- [23] M. Schmidt, F. M. Zimmer, and S. G. Magalhaes, *Phys. Scr.* **90**, 025809 (2015).
- [24] P. F. Godoy, M. Schmidt, and F. M. Zimmer, *Phys. Lett. A* **384**, 126687 (2020).
- [25] A. Sorokin, *Phys. A (Amsterdam, Neth.)* **602**, 127621 (2022).
- [26] R. M. Liu, W. Z. Zhuo, S. Dong, X. B. Lu, X. S. Gao, M. H. Qin, and J.-M. Liu, *Phys. Rev. E* **93**, 032114 (2016).
- [27] Y. Hu and P. Charbonneau, *Phys. Rev. B* **104**, 144429 (2021).
- [28] D. P. Landau and K. Binder, *Phys. Rev. B* **31**, 5946 (1985).
- [29] R. Subert and B. M. Mulder, *Phys. Rev. E* **106**, 014105 (2022).
- [30] A. R. Wildes, K. C. Rule, R. I. Bewley, M. Enderle, and T. J. Hicks, *J. Phys.: Condens. Matter* **24**, 416004 (2012).
- [31] D. Lançon, H. C. Walker, E. Ressouche, B. Ouladdiaf, K. C. Rule, G. J. McIntyre, T. J. Hicks, H. M. Rønnow, and A. R. Wildes, *Phys. Rev. B* **94**, 214407 (2016).
- [32] A. R. Wildes, D. Lançon, M. K. Chan, F. Weickert, N. Harrison, V. Simonet, M. E. Zhitomirsky, M. V. Gvozdkova, T. Ziman, and H. M. Rønnow, *Phys. Rev. B* **101**, 024415 (2020).
- [33] D. Yamamoto, G. Marmorini, M. Tabata, K. Sakakura, and I. Danshita, *Phys. Rev. B* **100**, 140410(R) (2019).
- [34] D. Yamamoto, G. Marmorini, and I. Danshita, *Phys. Rev. Lett.* **114**, 027201 (2015).
- [35] D. Yamamoto, G. Marmorini, and I. Danshita, *Phys. Rev. Lett.* **112**, 127203 (2014).
- [36] X. Z. Liu, O. Prokhnenko, D. Yamamoto, M. Bartkowiak, N. Kurita, and H. Tanaka, *Phys. Rev. B* **100**, 094436 (2019).
- [37] A. Singhanian and S. Kumar, *Phys. Rev. B* **98**, 104429 (2018).
- [38] A. Singhanian and S. Kumar, *Phys. Rev. B* **101**, 064403 (2020).
- [39] A. Krindges, C. Morais, M. Schmidt, and F. Zimmer, *J. Magn. Magn. Mater.* **577**, 170746 (2023).
- [40] Y.-Z. Ren, N.-H. Tong, and X.-C. Xie, *J. Phys.: Condens. Matter* **26**, 115601 (2014).
- [41] F. Zimmer, W. Silva, M. Schmidt, and S. Magalhaes, *J. Magn. Magn. Mater.* **554**, 169273 (2022).
- [42] M. Schmidt, G. Kohlrausch, and F. Zimmer, *Phys. A (Amsterdam, Neth.)* **596**, 127126 (2022).
- [43] G. L. K. Frantz, M. Schmidt, and F. M. Zimmer, *Phys. Rev. E* **103**, 032125 (2021).
- [44] M. Schmidt, N. Kellermann, and F. M. Zimmer, *Phys. Rev. E* **102**, 032139 (2020).
- [45] M. Schmidt and P. Godoy, *J. Magn. Magn. Mater.* **537**, 168151 (2021).
- [46] L. C. Rossato, F. Zimmer, C. Morais, and M. Schmidt, *Phys. A (Amsterdam, Neth.)* **621**, 128778 (2023).
- [47] P. F. Dias and M. Schmidt, *Phys. Rev. B* **108**, 014436 (2023).
- [48] A. I. Guerrero and S. Gaona J., *J. Magn. Magn. Mater.* **514**, 167140 (2020).
- [49] T. Balcerzak, K. Szałowski, A. Bobák, and M. Žukovič, *Phys. Rev. E* **98**, 022123 (2018).
- [50] R. Kaneko, Y. Douda, S. Goto, and I. Danshita, *J. Phys. Soc. Jpn.* **90**, 073001 (2021).
- [51] W. Selke, *Phys. Rep.* **170**, 213 (1988).
- [52] Y. Hu and P. Charbonneau, *Phys. Rev. B* **103**, 094441 (2021).
- [53] M. W. Butcher, M. A. Tanatar, and A. H. Nevidomskyy, *Phys. Rev. Lett.* **130**, 166701 (2023).
- [54] Q. H. Wang, A. Bedoya-Pinto, M. Blei, A. H. Dismukes, A. Hamo, S. Jenkins, M. Koperski, Y. Liu, Q.-C. Sun, E. J. Telford, H. H. Kim, M. Augustin, U. Vool, J.-X. Yin, L. H. Li, A. Falin, C. R. Dean, F. Casanova, R. F. L. Evans, M. Chshiev *et al.*, *ACS Nano* **16**, 6960 (2022).
- [55] J.-U. Lee, S. Lee, J. H. Ryoo, S. Kang, T. Y. Kim, P. Kim, C.-H. Park, J.-G. Park, and H. Cheong, *Nano Lett.* **16**, 7433 (2016).
- [56] R. Samajdar, W. W. Ho, H. Pichler, M. D. Lukin, and S. Sachdev, *Phys. Rev. Lett.* **124**, 103601 (2020).
- [57] P. Scholl, M. Schuler, H. J. Williams, A. A. Eberharter, D. Barredo, K.-N. Schymik, V. Lienhard, L.-P. Henry, T. C. Lang, T. Lahaye *et al.*, *Nature (London)* **595**, 233 (2021).